

Topological and geometric universal thermodynamics in conformal field theory

Hao-Xin Wang,^{1,*} Lei Chen,¹ Hai Lin,² and Wei Li^{1,3,†}

¹*Department of Physics, Key Laboratory of Micro-Nano Measurement-Manipulation and Physics (Ministry of Education), Beihang University, Beijing 100191, China*

²*Yau Mathematical Sciences Center, Tsinghua University, Beijing 100084, China*

³*International Research Institute of Multidisciplinary Science, Beihang University, Beijing 100191, China*



(Received 1 February 2018; revised manuscript received 1 June 2018; published 28 June 2018)

Universal thermal data in conformal field theory (CFT) offer a valuable means for characterizing and classifying criticality. With improved tensor network techniques, we investigate the universal thermodynamics on a nonorientable minimal surface, the crosscapped disk (or real projective plane, \mathbb{RP}^2). Through a cut-and-sew process, \mathbb{RP}^2 is topologically equivalent to a cylinder with rainbow and crosscap boundaries. We uncover that the crosscap contributes a fractional topological term $\frac{1}{2} \ln k$ related to a nonorientable genus, with k a universal constant in two-dimensional CFT, while the rainbow boundary gives rise to a geometric term $\frac{c}{4} \ln \beta$, with β the manifold size and c the central charge. We have also obtained analytically the logarithmic rainbow term by CFT calculations, and discuss its connection to the renowned Cardy-Peschel conical singularity.

DOI: [10.1103/PhysRevB.97.220407](https://doi.org/10.1103/PhysRevB.97.220407)

Introduction. Finding universal properties in the many-body system is very important for understanding critical phenomena [1–4], which constitutes a fascinating and influential topic in diverse fields of physics. According to two-dimensional (2D) conformal field theory (CFT) [5], universal terms appear in the thermodynamics of critical quantum chains at low temperatures [6], and 2D statistical models at the critical temperature. Among others, logarithmic corrections proportional to a ubiquitous central charge c are particularly interesting. Cardy and Peschel [4] showed that free energy contains logarithmic terms due to corners or bulk conical singularities [7–15]. This logarithmic term is universal and has profound ramifications in the studies of bipartite fidelity and quantum quenches of (1+1)D models [10,16], as well as in the corner entanglement entropy of (2+1)D quantum systems [17–20].

Recently, the universal thermodynamics of 2D CFTs on nonorientable surfaces has been explored, including the Klein bottle (\mathbb{K}^2) and Möbius strip [21–24]. For diagonal CFT partition functions on the Klein bottle, $F_{\mathcal{K}} = \ln \mathcal{Z}^{\mathcal{K}} = \frac{\pi c}{24v\beta} L + \ln k$, with a universal constant $k = \sum_a d_a / \mathcal{D}$, where d_a is the quantum dimension of the a th primary field, and $\mathcal{D} = \sqrt{\sum_a d_a^2}$ is the total quantum dimension.

In this Rapid Communication, we consider the real projective plane (\mathbb{RP}^2), whose elementary polygon is shown in Fig. 1(d). A specific realization of \mathbb{RP}^2 can be achieved by gluing a crosscap with a disk, along the open edge, i.e., a crosscapped disk as shown in Fig. 1(b). As a minimal surface, \mathbb{RP}^2 is a building block in constructing other nonorientable surfaces (e.g., \mathbb{K}^2). Therefore, exploring the possible universal CFT thermodynamics on \mathbb{RP}^2 is of particular interest.

Previous tensor network (TN) methods applied to \mathbb{K}^2 (say, in Ref. [23]) are not directly applicable to \mathbb{RP}^2 . Therefore, we devise here a boundary matrix product state (BMPS) approach to explore the residual free energy on \mathbb{RP}^2 . This BMPS technique is very efficient and can also improve the accuracy in extracting universal data on other nonorientable manifolds including \mathbb{K}^2 and Möbius strip, etc. The main idea is as follows: After a cut-and-sew process, \mathbb{RP}^2 is transformed into a plain cylinder with special conformal boundaries [Figs. 1(c) and 1(d)], one crosscap and one so-called rainbow state. We find the dominating eigenvector of the transfer matrix through an iterative method, and then extract the universal term by computing its overlap with the crosscap or rainbow boundaries.

With this efficient TN technique removing finite-size effects (in one spatial dimension out of two), as well as CFT analysis, we uncover two universal terms in CFT thermodynamics: the crosscap term $F_{\mathcal{C}} = \frac{1}{2} \ln k$, a fractional *topological* Klein bottle entropy due to twist operations; and a *geometric* rainbow term $F_{\mathcal{R}} = \frac{c}{4} \ln \beta$, as a consequence of the intrinsic “conical singularity” on \mathbb{RP}^2 , where c is the central charge and β the lattice width (or inverse temperature in quantum cases).

Models and TN representations. We perform TN simulations on the 2D statistical and (1+1)D quantum models. The statistical models include the Ising model $H = -\sum_{\langle i,j \rangle} s_i s_j$, where $s_i = \pm 1$; the three-state Potts $H = -\sum_{\langle i,j \rangle} \delta_{s_i, s_j}$, with $s_i = 0, 1, 2$, and δ the Kronecker delta function; and the Blume-Emery-Griffiths (BEG) [25] model $H = -\sum_{\langle i,j \rangle} s_i s_j + \Delta \sum_i s_i^2$ ($s_i = 0, \pm 1$). As shown in Fig. 2, we construct the partition-function TN by following either the original lattices where the models are defined [type I, Figs. 2(a) and 2(b)], or their “dual” lattices [type II, Figs. 2(c)–2(e)].

Type I TN contains vertex tensors T and bond matrices M . For instance, in Fig. 2(a), $T_{s_i, s_j, s_k, s_l} = 1$ (when $s_i = s_j = s_k = s_l$) or 0 (otherwise) is a generalized δ function, and the matrix $M_{s_m, s_n} = \exp(-h_{m,n}/T_c)$ stores the Boltzmann weight

* wanghaoxin@buaa.edu.cn

† w.li@buaa.edu.cn

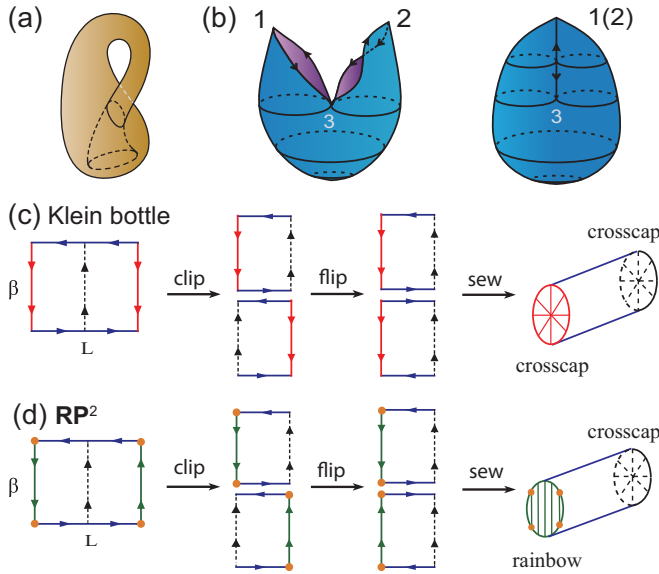


FIG. 1. Illustration of (a) the Klein bottle (\mathbb{K}^2) and (b) a crosscapped disk (right) obtained by gluing four lines pairwise with the arrows matched (left). (c), (d) show the cut-and-sew processes: One clips the elementary polygon vertically along the dashed line, flips the right half horizontally, and properly reglues the two pieces. \mathbb{K}^2 in (c) transforms into a flat cylinder with two crosscap boundaries, while in (d) \mathbb{RP}^2 there exist a crosscap and a rainbow. The two “branch” points labeled “1(2)” and “3” in (b), and correspondingly two pairs of orange sites in (d), play the role of effective conical singularities.

[$h_{m,n}$ is the interaction term on the (m,n) bond]. Hexagonal TN in Fig. 2(b) is constructed similarly, where T is of rank 3.

Type II TN consists of plaquettes/simplex tensors T . In Fig. 2(c), T tensors on (half of) the plaquettes connect each other via s indices and form a square-lattice TN. $T_{s_i, s_j, s_k, s_l} = \exp(-h_{\square_{i,j,k,l}}/T_c)$ and $h_{\square_{i,j,k,l}}$ is a plaquette Hamiltonian. Similarly, we can construct a hexagonal TN representation

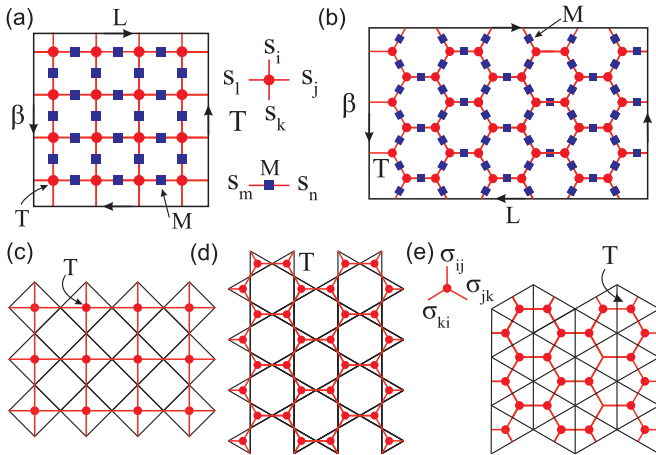


FIG. 2. Various lattice statistical models [(a), (c) square, (b) honeycomb, (d) kagome, and (e) triangular] and their corresponding TN representations. (a), (b) show TNs defined on the original lattices, and (c)–(e) defined on the “dual” lattices. To realize the \mathbb{RP}^2 manifold, we connect square TNs following the conventions in (a) and hexagonal TNs as in (b), such that the arrows match.

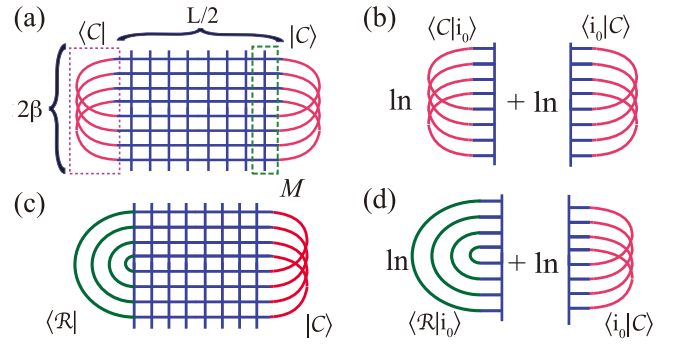


FIG. 3. (a) TN representation of the \mathbb{K}^2 partition function consists of columns of transfer matrices (M), capped with two crosscaps (C). The dominating eigenstate of M is denoted as $|i_0\rangle$. (b) The Klein term can be computed by summing over the logarithm of two overlaps. (c) By substituting one crosscap with a rainbow state $|\mathcal{R}\rangle$, one obtains in (d) the \mathbb{RP}^2 universal term.

for the kagome model in Fig. 2(d). For the triangular lattice in Fig. 2(e), the dual variables $\sigma_{ij} = s_i s_j$ (Ising) and $e^{2\pi i(s_i - s_j)/3}$ (Potts, see Ref. [26]) are introduced on each link (i, j) . Correspondingly, the simplex tensor $T_{\sigma_{ij}, \sigma_{jk}, \sigma_{ki}} = \exp(-h_{\Delta_{i,j,k}}/T_c) \delta_{\sigma_{ij}, \sigma_{jk}, \sigma_{ki}, 1}$, with $h_{\Delta_{i,j,k}} = -\frac{1}{2}(\sigma_{ij} + \sigma_{jk} + \sigma_{ki})$ (Ising) and $-\frac{1}{2}[\delta(\sigma_{ij}, 1) + \delta(\sigma_{jk}, 1) + \delta(\sigma_{ki}, 1)]$ (Potts).

Besides 2D statistical models, critical quantum chains include the transverse-field Ising [$H_{\text{TFI}} = \sum_i (-S_i^x S_{i+1}^x - \frac{1}{2} S_i^z)$], Heisenberg XY [$H_{\text{XY}} = -\sum_i (S_i^x S_{i+1}^x + S_i^y S_{i+1}^y)$], and \mathbb{Z}_3 quantum Potts [$H_{\text{Potts}} = -\sum_i (\sigma_i \sigma_{i+1}^\dagger + \tau_i) + \text{H.c.}$]. The local operators $S^{x,y,z}$ are spin-1/2 operators, and $\sigma_i = \text{diag}(1, \omega, \omega^2)$ with $\omega = e^{2\pi i/3}$, $\tau_i = (e_3, e_1, e_2)$. e_n is a unit column vector with only the n th element equal to 1 (others zero) [27]. Given the Hamiltonian H , the thermal TN representations of quantum chains can be obtained via the Trotter-Suzuki decomposition of $e^{-\beta H}$, which resemble Fig. 2(c).

As follows, we stick to the notation $L(\beta)$ for length (width) in terms of TNs, for both square-lattice [Figs. 2(a)

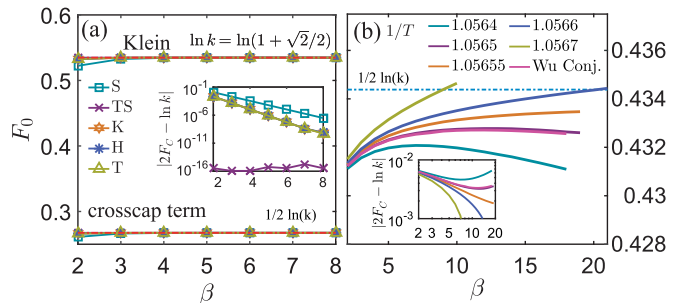


FIG. 4. (a) The Klein and crosscap terms of Ising models on various lattices. The crosscap term equals exactly one-half the Klein term. The inset shows the deviation of calculated F_K to the exact value. $D = 256$ bond states are retained in the BMPS, i.e., numerically exact. (b) shows F_C of the kagome Potts model at different temperatures, and the inset plots the deviation $|2F_C - \ln k|$. In this plot, Fig. 5, and Table I, “S” stands for square lattice, “TS” for the square lattice with tilted TN representation, “K” for kagome, “H” for honeycomb, and “T” for the triangular lattice.

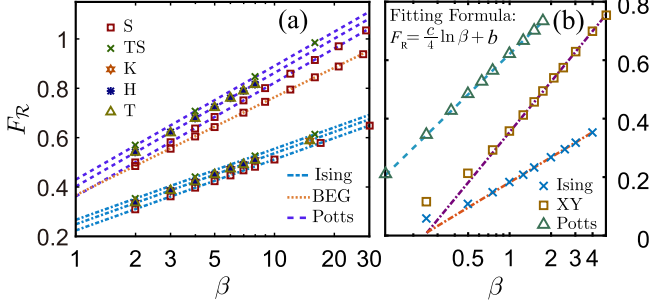


FIG. 5. Logarithmic rainbow terms of several critical (a) 2D statistical models and (b) quantum chains. For each model, $F_{\mathcal{R}}$ data collapse in three cases, i.e., on kagome, honeycomb, and triangular lattices.

and 2(c)] and honeycomb-lattice TNs [Figs. 2(b), 2(d) and 2(e)]. We always assume the thermodynamic limit $L \gg \beta \gg 1$, under which condition the relevant universal terms are well defined.

Efficient extraction of universal data. In previous TN studies [23], given a density operator ρ , we evaluate $\mathcal{Z}^{\mathcal{K}} = \text{Tr}[\Omega\rho(\beta)]$ (Ω is a spatial reflection operator) to extract universal data on the Klein bottle. The residual term $\ln k$ can then be obtained by computing the ratio $k = \frac{\mathcal{Z}^{\mathcal{K}}(2\beta, L/2)}{\mathcal{Z}^{\mathcal{T}}(\beta, L)}$, where $\mathcal{Z}^{\mathcal{T}}(\beta, L)$ is the torus partition function [21,22], or by extrapolating $\ln \mathcal{Z}^{\mathcal{K}}$ to $L = 0$ [23].

However, this scheme is not directly applicable to $\mathbb{R}\mathbb{P}^2$. Here, we propose a BMPS-based TN technique exploiting the cut-and-sew process in Fig. 1. Successive projections of the transfer matrix M [see Fig. 3(a)] to BMPS are performed to determine the (nondegenerate) dominant eigenvector $|i_0\rangle$ and then compute the universal data. In practice, 200–500 iterations suffice to converge the BMPS of bond dimension $D = 100$ –500, offering us results with high precision [28].

To be specific, we insert a complete set of orthonormal bases $\{|i_\mu\rangle\}$ into the partition function $\mathcal{Z}(\frac{L}{2}, 2\beta) = \langle \mathcal{B}_L | M^{L/2} | \mathcal{B}_R \rangle$, where μ counts the eigenstates $|i_\mu\rangle$ of the real symmetric transfer matrix M . We thus get $\mathcal{Z} = \sum_\mu \langle \mathcal{B}_L | i_\mu \rangle \lambda_\mu^{L/2} \langle i_\mu | \mathcal{B}_R \rangle$, in which only the dominant eigenvalue λ_0 and corresponding eigenvectors $|i_0\rangle$ survive in the thermodynamic limit, leading to $\ln \mathcal{Z} = \ln[\langle \mathcal{B}_L | i_0 \rangle \lambda_0^{L/2} \langle i_0 | \mathcal{B}_R \rangle] = \frac{L}{2} \ln \lambda_0 + F_0$. Clearly, the term $\frac{L}{2} \ln \lambda_0$ corresponds to the bulk free energy. Note the transfer matrix M is exactly the same as that of the Klein bottle

TABLE I. Fitted central charge c of 2D lattices (with z the coordination number) and 1D quantum chains (labeled as Q). For statistical models, c is fitted with the data of $\beta > 3$, while for quantum models c is fitted in the range $\beta > 1$. The numbers in parentheses represent the fitting error bar.

Model Lattice	Ising ($c = 0.5$)						BEG (0.7)		Potts (0.8)				XY (1)	
	S	TS	H	T	K	Q	S	S	TS	H	K	Q	Q	
T_c	$\cosh(2/T_c) \cos(\pi/z) = 1$ [32]						$\frac{4}{\ln(3+2\sqrt{3})}$ [33]	0.609 ^a	$\frac{1}{\ln(1+\sqrt{3})}$ [34]	0.6738 [34]	0.9465 ^b			
Slope	0.1250(2)	0.1250(2)	0.1250(1)	0.1250(1)	0.1250(1)	0.124(1)	0.172(1)	0.200(1)	0.200(1)	0.200(1)	0.199(1)	0.1996(5)	0.249(2)	
Fitted c	0.4998(8)	0.5000(7)	0.5000(1)	0.5000(1)	0.5000(1)	0.496(4)	0.688(4)	0.800(4)	0.798(2)	0.797(2)	0.804(3)	0.798(2)	0.996(8)	

^aFor the BEG model, the tricritical point corresponds to $\Delta = 1.966$ at $T_c = 0.609$ [28,35–38].

^bResults of this work; see Fig. 4(b).

(see Fig. 3), therefore the universal bulk correction is also $\frac{\pi c}{24\beta} L$ [23]. Besides, the residual term reads directly as

$$F_0 = \ln \langle \mathcal{B}_L | i_0 \rangle + \ln \langle i_0 | \mathcal{B}_R \rangle. \quad (1)$$

The cut-and-sew process transforms $\mathbb{R}\mathbb{P}^2$ into a cylinder with a crosscap $|\mathcal{C}\rangle$ and rainbow states $|\mathcal{R}\rangle$ on two ends, i.e., $\langle \mathcal{B}_L | = \langle \mathcal{R} |$ and $|\mathcal{B}_R \rangle = |\mathcal{C}\rangle$ [cf. Fig. 1(d)]. Therefore, the residual term $F_0 = F_C + F_{\mathcal{R}}$, where $F_C = \ln \langle i_0 | \mathcal{C} \rangle$ (crosscap term) and $F_{\mathcal{R}} = \ln \langle \mathcal{R} | i_0 \rangle$ (rainbow term).

Crosscap free-energy term. \mathbb{K}^2 is topologically equivalent to a cylinder with two crosscaps on the boundary, as shown in Figs. 1(c), 3(a), and 3(b). Therefore, $F_{\mathcal{K}} = \ln \langle \mathcal{C} | i_0 \rangle + \ln \langle i_0 | \mathcal{C} \rangle = \ln k$, and it is convenient to see that a fractional term $F_C = \frac{1}{2} \ln k$ constitutes an elementary unit of the topological term, associated with a single crosscap boundary $|\mathcal{C}\rangle$.

Figure 4(a) shows the Klein and crosscap terms of the Ising model on various lattices, which converge to the values $F_{\mathcal{K}} = \ln(1 + \sqrt{2}/2)$ and $F_C = \frac{1}{2} F_{\mathcal{K}}$, respectively. The latter relation is also consistent with the CFT predictions of the $\mathbb{R}\mathbb{P}^2$ partition function [29]. In particular, one can observe that F_C data converge exponentially fast toward the universal CFT value as β increases, regardless of the specific lattice geometries, or even remain identical with $\frac{1}{2} \ln k$ up to machine precision [TS case in Fig. 4(a)].

As a useful application, we show that F_C can be employed to accurately determine the critical points, even for challenging models such as the three-state kagome Potts and square-lattice BEG models [28]. In Fig. 4(b) we show the results for kagome Potts: When T approaches critical temperature T_c , F_C converges to $\frac{1}{2} \ln k$ ($k = \sqrt{3 + \frac{6}{\sqrt{5}}}$), which otherwise deviates from the universal value. Therefore, from distinct behaviors of the F_C curves [see $|2F_C - \ln k|$ in the inset of Fig. 4(b)], we can pinpoint the critical temperature as $1/T_c \simeq 1.05655(5)$. This value constitutes a rather accurate estimate of T_c , which is in very good agreement with $1/T_c = 1.05656(2)$ estimated in Ref. [30], as well as $1.0565602231(1)$ in Ref. [31].

The crosscap term deeply relates to topology. Based on the above observation for $\mathbb{R}\mathbb{P}^2$, as well as that in the Möbius-band case [23], we conjecture that manifolds with a nonorientable genus κ (i.e., with κ crosscaps) give rise to a universal topological term $\frac{\kappa}{2} \ln k$.

The rainbow free-energy term. Besides the constant crosscap contribution, there exists another logarithmic term in the $\mathbb{R}\mathbb{P}^2$ free energy due to the rainbow boundary $|\mathcal{R}\rangle$, i.e.,

$$F_{\mathcal{R}} = \frac{c}{4} \ln \beta + b, \quad (2)$$

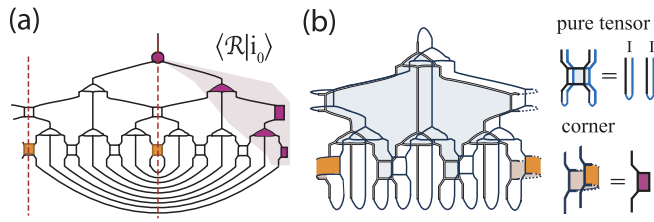


FIG. 6. (a) Overlap $\langle \mathcal{R}|i_0 \rangle$ of the rainbow state with the scale-invariant MERA can be translated into a folded MERA in (b), where the pure tensors (isometries and unitaries) cancel each other into identities, while the “corner” tensors are folded by themselves [right down in (b), coinciding double lines of the original tensor are combined into single indices of the folded one] and located within the boundary causal cone again shown in (a).

where c is the central charge, and b is the nonuniversal constant. In Fig. 5, we show that, for both 2D statistical models (Ising, Potts, BEG) and 1D critical quantum chains (Ising, Potts, and XY), the rainbow term scales logarithmically versus β . The central charge c can be fitted from the slope, and the results are summarized in Table I, where a perfect agreement with CFT is observed.

Universal logarithmic terms often appear on lattice geometries with corners (such as open strips [4,12,13]), conical singularities [8], or even a slit [10,14]. Although $\mathbb{R}P^2$ is a closed manifold without any corners or conical angles, a closer look into the lattice geometry in Fig. 1(d) [and Figs. 3(c) and 3(d)] reveals that there exist two pairs of points which are connected twice by lattice bonds (and thus identified twice in the continuous limit), forming effective “conical singularities” on the rainbow boundary. These intrinsic conical points are responsible for the logarithmic term on $\mathbb{R}P^2$.

We provide an intuitive explanation with the multiscale entanglement renormalization ansatz (MERA) [39], i.e., a holographic view. As shown in Fig. 6(a), the dominant eigenvector $|i_0 \rangle$ of the transfer matrix is a critical quantum state, which has a scale-invariant MERA representation consisting of rank-4 unitary and rank-3 isometry tensors. Following the rainbow boundary condition, we fold MERA along two vertical lines and arrive at a double “MERA” in Fig. 6(b). Due to the reflection symmetry, the isometry and unitary tensors in the bulk cancel into identities and do not contribute in $\langle \mathcal{R}|i_0 \rangle$, while only the “corner” tensors (due to folding) contribute to

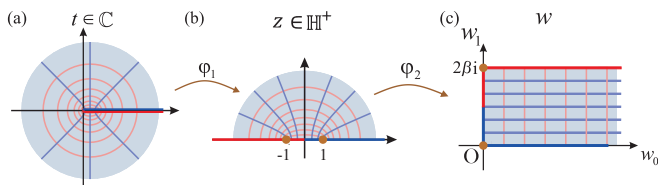


FIG. 7. The conformal transformation $\varphi_1 : z = \sqrt{t}$ maps (a) the complex plane to (b) the upper half plane, which is then mapped onto a semi-infinite rectangle via the Schwarz-Christoffel transformation $\varphi_2 : w = \frac{2\beta}{\pi} \text{arcosh}(z)$. Fields defined on the complex plane are assumed to take the same values on the highlighted red and blue lines, giving rise to a rainbow and cylindrical boundary conditions in (c).

TABLE II. Nonorientable universal thermodynamics F_0 .

Manifolds	Klein bottle	Möbius strip	$\mathbb{R}P^2$
κ	2	1	1
η	1	1/2	1/2
μ	0	0	$c/4$
ν	$\pi c/24$	$\pi c/24$	$\pi c/24$

the final trace. Note that on the lowest row of MERA the two self-folded corner tensors (colored orange) connect the four special “corner” sites indicated in Fig. 1(d). Besides the two corner tensors in the physical layer, there exist $O(\ln \beta)$ such “self-folded” boundary tensors, constrained in the past causal cone [dashed region shown in Fig. 6(a)] of MERA. Each boundary “impurity” contributes the same factor due to the scale invariance, and thus $\langle \mathcal{R}|i_0 \rangle \sim a^{\ln \beta}$ (i.e., $\sim \beta^\gamma$), giving rise to a logarithmic “corner” term $F_{\mathcal{R}} \sim \ln \beta$.

CFT analysis of the rainbow term. We also analytically derive the rainbow term [28] by noting the two successive transformations (φ_1 and φ_2 in Fig. 7). They map the complex plane to a half-infinite cylinder with a rainbow state on segment $[0, 2i\beta]$ in Fig. 7(c), where $\varphi_2(-1) = 2\beta i$ and $\varphi_2(1) = 0$. Neglecting the nonuniversal term and assuming $\langle T(t) \rangle = 0$, we obtain $\langle T(w) \rangle = -\frac{c\pi^2}{8(2\beta)^2} \left[\frac{\sinh^2(\pi w/2\beta)}{\cosh^2(\pi w/2\beta)} + \frac{\cosh^2(\pi w/2\beta)}{\sinh^2(\pi w/2\beta)} \right] + \frac{c\pi^2}{12(2\beta)^2}$ according to the transformation of the stress tensor. As the metric tensor $g_{\mu\nu}$ changes with a tiny variable $\delta g_{\mu\nu} = 2\epsilon \delta_{\mu 1} \delta_{\nu 1}$, the logarithm of the partition function (denoted as F_0) varies as $\delta F_0 = \frac{1}{2} \int d^2x \sqrt{g} \delta g_{\mu\nu} \langle T^{\mu\nu} \rangle = \frac{1}{\pi} \int_0^{2\beta} dw^1 \int_{iw^1}^{L/2+iw^1} dw^0 \langle T(w) \rangle \frac{\delta\beta}{\beta}$. We integrate it and arrive at the universal term $F_0 = \frac{\pi cL}{24\beta} + \frac{c}{4} \ln \beta$. The first term $\frac{\pi cL}{24\beta}$ also appears in the Klein bottle and Möbius strip cases [21–23], as a consequence of the nonorientability for these manifolds. The second $\frac{c}{4} \ln \beta$ is the logarithmic rainbow free-energy term we have observed numerically.

Discussion and summary. The logarithmic rainbow term is geometry dependent and can be related to the renowned Cardy-Peschel conical singularity term $F_0(\theta) = \frac{c\theta}{24\pi} \left[\left(\frac{2\pi}{\theta} \right)^2 - 1 \right] \ln L$, with L the characteristic system size. Due to the particular lattice realization of $\mathbb{R}P^2$ as in Figs. 2(a) and 2(b), there exist two effective π -angle conical singularities in the TN [see Fig. 1(d)], which in total contribute $2F_0(\pi) = \frac{c}{4} \ln \beta$ (with $\beta \sim L$). Note that the conical angle changes as we alter the specific geometry of the $\mathbb{R}P^2$ TN, which introduces a multiplicative geometric factor, following the Cardy-Peschel formula above [28].

In Table II, we briefly summarize the results on nonorientable universal thermodynamics, in the form $F_0 = \eta \ln k + \mu \ln \beta + \nu L/\beta$. Remarkably, the coefficient γ is proportional to the nonorientable genus κ of the surface, i.e., a topological term, and μ scales linearly with the central charge c , with a geometry-dependent slope. More connections of these universal data to topology and geometry deserve further investigations.

Acknowledgments. The authors are indebted to Jin Chen, Xintian Wu, Lei Wang, and Hong-Hao Tu for stimulating discussions. This work was supported by the National Natural Science Foundation of China (Grant No. 11504014).

- [1] I. Affleck, Universal Term in the Free Energy at a Critical Point and the Conformal Anomaly, *Phys. Rev. Lett.* **56**, 746 (1986).
- [2] H. W. J. Blöte, J. L. Cardy, and M. P. Nightingale, Conformal Invariance, the Central Charge, and Universal Finite-Size Amplitudes at Criticality, *Phys. Rev. Lett.* **56**, 742 (1986).
- [3] I. Affleck and A. W. W. Ludwig, Universal Noninteger “Ground-State Degeneracy” in Critical Quantum Systems, *Phys. Rev. Lett.* **67**, 161 (1991).
- [4] J. Cardy and I. Peschel, Finite-size dependence of the free energy in two-dimensional critical systems, *Nucl. Phys. B* **300**, 377 (1988).
- [5] P. D. Francesco, P. Mathieu, and D. Sènèchal, *Conformal Field Theory* (Springer, New York, 1997).
- [6] S. Sachdev, *Quantum Phase Transitions* (Cambridge University Press, Cambridge, U.K., 2011).
- [7] P. Kleban and I. Vassileva, Free energy of rectangular domains at criticality, *J. Phys. A: Math. Gen.* **24**, 3407 (1991).
- [8] R. Costa-Santos, Logarithmic corrections to the Ising model free energy on lattices with conical singularities, *Phys. Rev. B* **68**, 224423 (2003).
- [9] E. Vernier and J.-L. Jacobsen, Corner free energies and boundary effects for Ising, Potts and fully packed loop models on the square and triangular lattices, *J. Phys. A: Math. Theor.* **45**, 045003 (2012).
- [10] J.-M. Stéphan and J. Dubail, Logarithmic corrections to the free energy from sharp corners with angle 2π , *J. Stat. Mech.: Theory Exp.* (2013) P09002.
- [11] R. Bondesan, J. Dubail, J. L. Jacobsen, and H. Saleur, Conformal boundary state for the rectangular geometry, *Nucl. Phys. B* **862**, 553 (2012).
- [12] X. Wu, N. Izmailian, and W. Guo, Finite-size behavior of the critical Ising model on a rectangle with free boundaries, *Phys. Rev. E* **86**, 041149 (2012).
- [13] X. Wu, N. Izmailian, and W. Guo, Shape-dependent finite-size effect of the critical two-dimensional Ising model on a triangular lattice, *Phys. Rev. E* **87**, 022124 (2013).
- [14] X. Wu, Critical behavior of the two-dimensional Ising model with a slit, *Phys. Rev. E* **95**, 052101 (2017).
- [15] J.-M. Stéphan, Emptiness formation probability, Toeplitz determinants, and conformal field theory, *J. Stat. Mech.: Theory Exp.* (2014) P05010.
- [16] J. Dubail and J.-M. Stéphan, Universal behavior of a bipartite fidelity at quantum criticality, *J. Stat. Mech.: Theory Exp.* (2011) L03002.
- [17] E. Fradkin and J. E. Moore, Entanglement Entropy of 2D Conformal Quantum Critical Points: Hearing the Shape of a Quantum Drum, *Phys. Rev. Lett.* **97**, 050404 (2006).
- [18] E. M. Stoudenmire, P. Gustainis, R. Johal, S. Wessel, and R. G. Melko, Corner contribution to the entanglement entropy of strongly interacting O(2) quantum critical systems in 2+1 dimensions, *Phys. Rev. B* **90**, 235106 (2014).
- [19] P. Bueno, R. C. Myers, and W. Witczak-Krempa, Universality of Corner Entanglement in Conformal Field Theories, *Phys. Rev. Lett.* **115**, 021602 (2015).
- [20] M. P. Zaletel, J. H. Bardarson, and J. E. Moore, Logarithmic Terms in Entanglement Entropies of 2D Quantum Critical Points and Shannon Entropies of Spin Chains, *Phys. Rev. Lett.* **107**, 020402 (2011).
- [21] H.-H. Tu, Universal Entropy of Conformal Critical Theories on a Klein Bottle, *Phys. Rev. Lett.* **119**, 261603 (2017).
- [22] W. Tang, L. Chen, W. Li, X. C. Xie, H.-H. Tu, and L. Wang, Universal boundary entropies in conformal field theory: A quantum Monte Carlo study, *Phys. Rev. B* **96**, 115136 (2017).
- [23] L. Chen, H.-X. Wang, L. Wang, and W. Li, Conformal thermal tensor network and universal entropy on topological manifolds, *Phys. Rev. B* **96**, 174429 (2017).
- [24] W. Tang, X. C. Xie, L. Wang, and H.-H. Tu, The Klein bottle entropy of the compactified boson conformal field theory, [arXiv:1805.01300](https://arxiv.org/abs/1805.01300).
- [25] M. Blume, V. J. Emery, and R. B. Griffiths, Ising model for the λ transition and phase separation in He³-He⁴ mixtures, *Phys. Rev. A* **4**, 1071 (1971).
- [26] M.-X. Wang, J.-W. Cai, Z.-Y. Xie, Q.-N. Chen, H.-H. Zhao, and Z.-C. Wei, Investigation of the Potts model on triangular lattices by the second renormalization of tensor network states, *Chin. Phys. Lett.* **27**, 076402 (2010).
- [27] W. Li, S. Yang, H.-H. Tu, and M. Cheng, Criticality in translation-invariant parafermion chains, *Phys. Rev. B* **91**, 115133 (2015).
- [28] See Supplemental Material at <http://link.aps.org/supplemental/10.1103/PhysRevB.97.220407> for detailed CFT calculations of the rainbow free-energy term (Sec. I), TN arithmetics (Sec. II), determination of the BEG model transition point (Sec. III), as well as discussions on different conical angles in \mathbb{RP}^2 TN realizations and their effects on universal terms (Sec. IV).
- [29] A. Maloney and S. F. Ross, Holography on non-orientable surfaces, *Classical Quantum Gravity* **33**, 185006 (2016).
- [30] I. Jensen, A. J. Guttmann, and I. G. Enting, The Potts model on kagome and honeycomb lattices, *J. Phys. A: Math. Gen.* **30**, 8067 (1997).
- [31] C. R. Scullard and J. L. Jacobsen, Potts-model critical manifolds revisited, *J. Phys. A: Math. Gen.* **49**, 125003 (2016).
- [32] G. H. Wannier, Antiferromagnetism. The triangular Ising net, *Phys. Rev.* **79**, 357 (1950).
- [33] K. Kanô and S. Naya, Antiferromagnetism. The kagome Ising net, *Prog. Theor. Phys.* **10**, 158 (1953).
- [34] F. Y. Wu, The Potts model, *Rev. Mod. Phys.* **54**, 235 (1982).
- [35] W. Kwak, J. Jeong, J. Lee, and D.-H. Kim, First-order phase transition and tricritical scaling behavior of the Blume-Capel model: A Wang-Landau sampling approach, *Phys. Rev. E* **92**, 022134 (2015).
- [36] C. J. Silva, A. A. Caparica, and J. A. Plascak, Wang-Landau Monte Carlo simulation of the Blume-Capel model, *Phys. Rev. E* **73**, 036702 (2006).
- [37] R. da Silva, N. A. Alves, and J. R. Drugowich de Felício, Universality and scaling study of the critical behavior of the two-dimensional Blume-Capel model in short-time dynamics, *Phys. Rev. E* **66**, 026130 (2002).
- [38] A. N. Berker and M. Wortis, Blume-Emery-Griffiths-Potts model in two dimensions: Phase diagram and critical properties from a position-space renormalization group, *Phys. Rev. B* **14**, 4946 (1976).
- [39] G. Vidal, Entanglement Renormalization, *Phys. Rev. Lett.* **99**, 220405 (2007); G. Evenbly and G. Vidal, Algorithms for entanglement renormalization, *Phys. Rev. B* **79**, 144108 (2009).